Article ID: 1000-7032(2024)12-2021-09

Energy Transfer and Photoluminescence Enhancement in WS_2/hBN/MoS_2 Heterostructures

CHEN Pengyao[1], REN Bingyan[1], ZHANG Chengyu[1], LI Boyuan[2], WANG Jiaxi[1], ZHANG Kaixuan[1], ZHAO Weijie[1,3*]

(1. *School of Physics, Southeast University, Nanjing* 211189, *China*;
2. *Chien-Shiung Wu College, Southeast University, Nanjing* 211102, *China*;
3. *Purple Mountain Laboratories, Nanjing* 211111, *China*)
* *Corresponding Author, E-mail: zhaowj@seu.edu.cn*

Abstract: Two-dimensional(2D) transition metal dichalcogenides(TMDs) and their heterostructures(HSs) exhibit unique optical properties and show great promise for developing next-generation optoelectronics. However, the photoluminescence(PL) quantum yield of monolayer(1L) TMDs is still quite low at room temperature, which severely limits their practical applications. Here we report a PL enhancement effect of 1L WS_2 at room temperature when constructing it into 1L-WS_2/hBN/1L-MoS_2 vertical HSs. The PL enhancement factors(EFs) can be up to 4.2. By using transient absorption(TA) spectroscopy, we demonstrate that the PL enhancement effect is due to energy transfer from 1L MoS_2 to 1L WS_2. The energy transfer process occurs on a picosecond timescale and lasts more than one hundred picoseconds which indicates a prominent contribution from exciton-exciton annihilation. Furthermore, the PL enhancement effect of 1L WS_2 can be observed in 2L-MoS_2/hBN/1L-WS_2 and 3L-MoS_2/hBN/1L-WS_2 HSs. Our study provides a comprehensive understanding of the energy transfer process in the PL enhancement of 2D TMDs and a feasible way to optimize the performance of TMD-based optoelectronic devices.

Key words: transition metal dichalcogenide; van der Waals heterostructures; photoluminescence; Förster resonance energy transfer; exciton-exciton annihilation

CLC number: O482.31 **Document code**: A **DOI**: 10.37188/CJL.20240238

WS_2/hBN/MoS_2异质结中的能量转移和光致发光增强

陈朋尧[1], 任冰燕[1], 张丞昱[1], 李博远[2], 王嘉熙[1], 张凯旋[1], 赵伟杰[1,3*]

(1.东南大学 物理学院, 江苏 南京 211189; 2.东南大学 吴健雄学院, 江苏 南京 211102;
3.紫金山实验室, 江苏 南京 211111)

摘要: 二维过渡金属二硫族化合物(TMDs)及其异质结具有独特的光学特性,因此在发展下一代光电器件方面具有广阔的应用前景。但是,在室温下单层(1L)过渡金属二硫族化合物的光致发光效率非常低,这严重阻碍了其在光电器件中的实际应用。本文报道了一种增强单层TMDs的光致发光效率的有效方法,即通过构建1L-WS_2/hBN/1L-MoS_2垂直异质结,能够大幅提升单层WS_2的光致发光效率,其增强因子最高可达4.2。利用瞬态吸收光谱,我们验证了该荧光增强效应是由1L MoS_2向1L WS_2的能量转移引起的。能量传递过程发生在皮秒时间尺度上,但其持续时间超过100 ps,这表明激子-激子湮灭对能量转移有重要影响。此外,在2L-MoS_2/hBN/1L-WS_2和3L-MoS_2/hBN/1L-WS_2异质结中,我们均能观察到单层WS_2的荧光增强效应。本研究为深入理解二维TMDs异质结中的能量转移机制打下了良好的基础,并为优化基于TMDs异质结的光电器件性能提供了可行方案。

关 键 词: 过渡金属硫族化合物; 范德瓦尔斯异质结; 光致发光; 共振能量转移; 激子-激子湮灭

收稿日期: 2024-09-29; **修订日期**: 2024-10-14
基金项目: 江苏省基础研究计划自然科学基金——前沿引领技术基础研究专项(BK20222007)
Supported by Natural Science Foundation of Jiangsu Province, Major Project(BK20222007)

1 Introduction

Two-dimensional group Ⅵ transition metal dichalcogenides (TMDs) such as WS_2 and MoS_2, have attracted significant research attention for their distinctive properties[1-3] and promising optoelectronic applications[4-7]. In monolayer and few-layer TMDs, the reduced dielectric screening and strong Coulomb attraction between electrons and holes allow to form tightly bound excitons with large binding energy at room temperature[6-11]. In particular, monolayer TMDs have a direct band gap at the high symmetry K/K' points of the Brillouin zone[3,12] and thus could have high photoluminescence quantum yield (PLQY)[13]. These optical properties make TMDs hold great potential for investigating fascinating properties of excitons at high temperature and developing light-emitting devices. However, mechanically exfoliated[14] or CVD-prepared[15] 1L TMDs usually exhibit low PLQY, typically ranging from 0.001% to 5%[16], which is mainly due to the presence of structural defects and many-body effects (trion formation, exciton-exciton annihilation, *etc*)[17-25].

A variety of approaches have been developed to improve the PLQY of 1L TMDs, such as chemical treatment[26], strain engineering[27], laser treatment[28] and hBN encapsulation[29-30]. Among these approaches, chemical treatment *via* trifluoromethanesulfonimide (H-TFSI)[26] or oleic acid (OA)[31] has been used to improve PLQY substantially. However, the use of those acids is not ideal for practical applications in optoelectronic devices because of their potential damage to TMDs materials and electrical contacts. 1L TMDs encapsulated with hBN show suppressed exciton-exciton annihilation (EEA) and homogeneous exciton PL spectra at high excitation intensity consequently. However, the hBN encapsulation does not markedly enhance PLQY at low excitation densities. In addition, monolayer TMDs can be integrated with different bulk or 2D materials to form type Ⅰ or type Ⅱ heterostructures (HSs) such as MoS_2/ZnO[32], WS_2/hBN/$MoSe_2$[33], $MoSe_2$/ReS_2[34]. The PLQY of TMDs in these HSs can be enhanced *via* the interlayer charge transfer (CT) or energy transfer (ET).

The interlayer CT results from the electronic band offset between different TMDs in HSs, and its efficiency highly depends on the interlayer distance. Meanwhile, the interlayer ET shows two different mechanisms, *i. e.*, the Förster resonance energy transfer (FRET) and Dexter energy transfer (DET). The FRET process[35-36] refers to the transport of electronic energy from the donor to the acceptor *via* dipole-dipole coupling, and it can occur at a relatively long distance (up to a few tens of nanometers). In contrast, the DET[35] is based on electron exchange and happens only in close proximity (within a few nanometers), similar to the CT process. Previous studies have demonstrated that the FRET is more effective than the DET and CT to improve the PLQY[33-34] of 1L TMDs in their HSs. The FRET process can be affected by the interlayer distance (θ) and spectral overlap between donor-type and acceptor-type TMDs[34]. Therefore, the PLQY of 1L TMDs is expected to be significantly enhanced by a proper selection of TMDs combinations and a prudent design of their HSs.

In this work, we choose 1L WS_2, exhibiting higher PLQY than other monolayer group Ⅵ TMDs[28], and build it into 1L-WS_2/hBN/1L-MoS_2 HSs. Since the B exciton resonance of 1L MoS_2 (donor) strongly overlaps with the A exciton resonance of 1L WS_2 (acceptor), efficient interlayer ET is observed and results in up to 4.2-fold PL enhancement of 1L WS_2 in the HSs at room temperature. Moreover, significant PL enhancement of 1L WS_2 can also be achieved in 2L-MoS_2/hBN/1L-WS_2 and 3L-MoS_2/hBN/1L-WS_2 HSs. By exploiting ultrafast transient absorption spectroscopy (TA), we observed that the FRET process occurred on a picosecond timescale, and lasted for more than one hundred picosecond (ps) owing to exciton-exciton annihilation. Our findings provide a comprehensive understanding of the FRET in improving the light-emission efficiency of 2D TMDs and pave the way for developing high-performance optoelectronic devices.

2 Experiment

2.1 Fabrication of Heterostructure

HSs were fabricated using the PDMS-based dry

transfer technique. Monolayer TMDs and thin hBN flakes were mechanically exfoliated from bulk crystals onto PDMS films and then transferred layer-by-layer onto quartz substrate in a nitrogen-filled glovebox. After transfer processes, 1L-MoS_2/hBN/1L-WS_2, 1L-WS_2/hBN/1L-MoS_2 and hBN/1L-MoS_2/1L-WS_2 HSs were annealed at 200 ℃ for 2 h to remove as much polymer residue as possible and make the stacked flakes in good contact with each other.

2.2 Characterizations

We used an MFP-3D atomic force microscopy (AFM) to obtain the high-resolution AFM image. The differential reflectance, Raman and PL measurements were performed using Jobin-Yvon HR800 micro-Raman spectrometer. A tungsten-halogen lamp was used as the light source. The differential reflectance spectra are defined by $(R_{sample} - R_{substrate})/R_{substrate}$. The CW solid-state 532 nm and 785 nm lasers and a 50× objective lens were used for single-shot spectroscopy measurements at room temperature. PL mapping was conducted using the XploRA Plus micro-Raman spectrometer, and the optical signals were collected with a 100× objective.

For femtosecond TA spectroscopy, the femtosecond pulsed laser (FemtoYL® -Vary, 1 030 nm, ~ 400 fs) was split into to two light beams using a beamsplitter. One beam goes through a beta barium borate (BBO) crystal to generate the pump laser (515 nm). The other beam was focused onto a YAG crystal to produce the probe pulses covering a broad range from 450 nm to 680 nm. A high-resolution motorized delay stage was used to control the delay time between the pump pulse and the probe pulse. And both beams were focused onto the samples using an objective lens. The transmitted probe beam was recorded at various delay time.

3 Results and Discussion

Fig. 1(a) displays the optical image of a HS sample. To eliminate the effect of interlayer CT, an approximately 8 nm thick hBN (see Supporting Information, Fig. S1) serves as a barrier layer between 1L MoS_2 and 1L WS_2. The crystal structures of this HS sample are illustrated in Fig. 1(b). Raman spectra are obtained at room temperature with a 1.58 eV (785 nm) excitation for individual 1L MoS_2, 1L WS_2, and the 1L-MoS_2/hBN/1L-WS_2 HS, respectively, as shown in Fig. 1(c). The characteristic Raman modes E^1_{2g} (360 cm^{-1}) and A_{1g} (420 cm^{-1}) correspond to the in-plane and out-of-plane lattice vibrations for 1L WS_2, respectively. For 1L MoS_2, E^1_{2g} is observed at 386 cm^{-1}, while A_{1g} is at 406 cm^{-1}, agreeing well with the literature[37]. The Raman spectrum of the HS shows four vibration modes, which are consistent with those of individual 1L MoS_2 and 1L WS_2, suggesting the high quality of this HS sample.

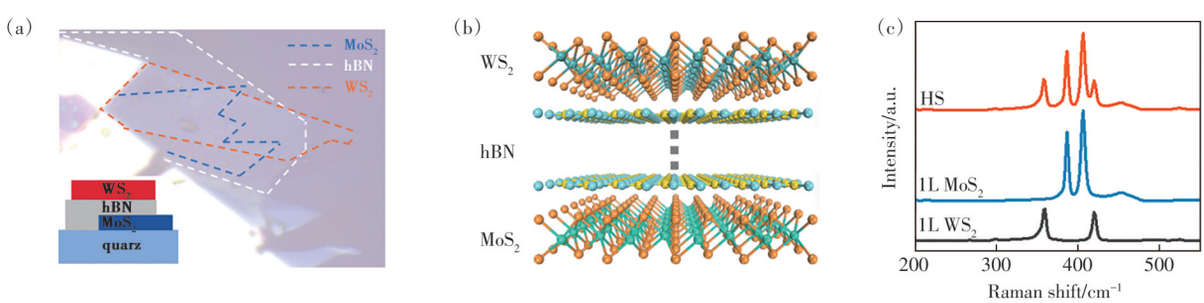

Fig. 1　(a) Optical image of a 1L-MoS_2/hBN/1L-WS_2 heterostructure (HS). The orange, white and blue line areas are 1L WS_2, hBN and 1L MoS_2, respectively. (b) The schematic structure of the HS sample. (c) Raman spectra of 1L WS_2, 1L MoS_2 and their HS measured with a 785 nm excitation

The differential reflectance spectra of 1L WS_2, 1L MoS_2, and the HS shown in Fig. 2(a) are defined by $(R_{sample} - R_{substrate})/R_{substrate}$, where R_{sample} and $R_{substrate}$ represent the reflected light intensities of the samples and the quartz substrate, respectively. The differential reflectance spectra for few-layer TMD on a transparent substrate can be related to its absorbance spectrum[34]. The A exciton absorption peak of 1L WS_2 is centered at 2.0 eV[38]. For 1L MoS_2, the peak at 1.90 eV and the broad peak centered at

2.04 eV correspond to A exciton and B exciton, respectively[39]. Compared to 1L MoS_2 and WS_2, the redshift of exciton absorption peaks in the HS is due to change of dielectric environment[40]. Most importantly, the strong spectral overlap between B exciton of 1L MoS_2 and A exciton of 1L WS_2 shown in Fig. 2(a) could facilitate the interlayer FRET between them.

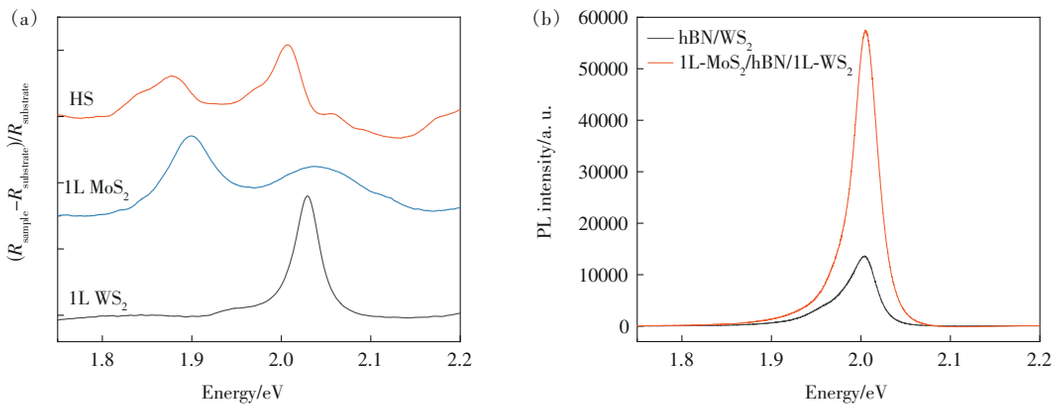

Fig. 2 (a) Differential reflectance spectra of 1L WS_2, 1L MoS_2 and their HS at room temperature. (b) PL spectra of 1L WS_2 on hBN and in the HS region at room temperature measured with a 532 nm excitation

PL spectra of 1L WS_2 and 1L-MoS_2/hBN/1L-WS_2 HSs at room temperature (RT) are presented in Fig. 2(b). Indeed, the PL intensity of 1L-WS_2 A exciton in the HS is enhanced by a factor of ~4.2 compared to that of individual WS_2 under the same experimental conditions. The PLQY of 1L MoS_2 is two orders of magnitude lower than that of 1L WS_2 (Fig. S2), and therefore its PL spectrum is barely visible in Fig. 2(b). In Fig. S3, we show that the PL peak of 1L MoS_2 B excitons overlaps with the absorption peak of 1L WS_2 A exciton, which is ideal for efficient FRET process. In addition, we show that the PL enhancement effect is robust at the HS region by using PL mapping and excitation-power dependent PL measurements in Fig. S4. The PL peak of 1L WS_2 in the HS region did not show notable redshift with increasing excitation power, indicating that the heating effect from laser excitations is negligible.

In order to understand the underlying physics of this PL enhancement effect, we consider various possible mechanisms. First, the PL contribution of B excitons in 1L MoS_2 is excluded as it is three orders of magnitude lower than that of A exciton of 1L WS_2 under the same excitation conditions shown in Fig. 2(b) and Fig. S2. Secondly, the interference effect and change of the dielectric environment of 1L WS_2 are ruled out by checking HSs with different stacking order, namely for 1L WS_2 as the top or bottom layer (Fig. S5). Thirdly, the hBN/1L-MoS_2/1L-WS_2 HS is demonstrated to show strongly suppressed PL of 1L WS_2 at the HS region as a result of interlayer charge transfer (Fig. S6), in agreement with previous results[41]. Furthermore, the DET occurs in a short-range interlayer distance (≤1 nm) and in type I HSs[35]. Therefore, the interlayer FRET from B excitons of 1L MoS_2 to A excitons of 1L WS_2 is the most possible mechanism for this PL enhancement effect.

TA measurements were conducted to gain more insights of FRET in 1L-MoS_2/hBN/1L-WS_2 HSs. A femtosecond laser pulse at a wavelength of 515 nm serves as the pump beam to excite samples, while a white-light probe pulse is used to monitor the change of absorption as a function of delay times. The pump fluence was kept at relatively low power to avoid any possible damage to samples. The color plot of TA spectra of 1L WS_2, the HS and 1L MoS_2 region are shown in Fig. 3(a)-(c), respectively. For individual 1L WS_2, a prominent ground state bleaching (GSB) signal centered at ~2.03 eV is observed and mainly attributed to photogenerated exciton population[42-44]. The TA spectra of 1L MoS_2 show two GSB features centered at ~1.90 eV and ~2.04 eV corresponding to its A and B excitons[42], respectively. It is worthy of mention that the GSB intensity of A and B

excitons in 1L MoS_2 is about one order of magnitude smaller than that of A excitons of 1L WS_2 under the same experimental conditions, which is probably due to the high defect density in MoS_2 exfoliated from natural crystals[45]. Consequently, the TA spectra of the HS region is dominated by the GSB of A excitons of 1L WS_2 in Fig. 3(b). In Fig. 3(d), the TA spectra of the HS region extracted at 2.1 ps are almost a simple sum of those of individual 1L MoS_2 and 1L WS_2.

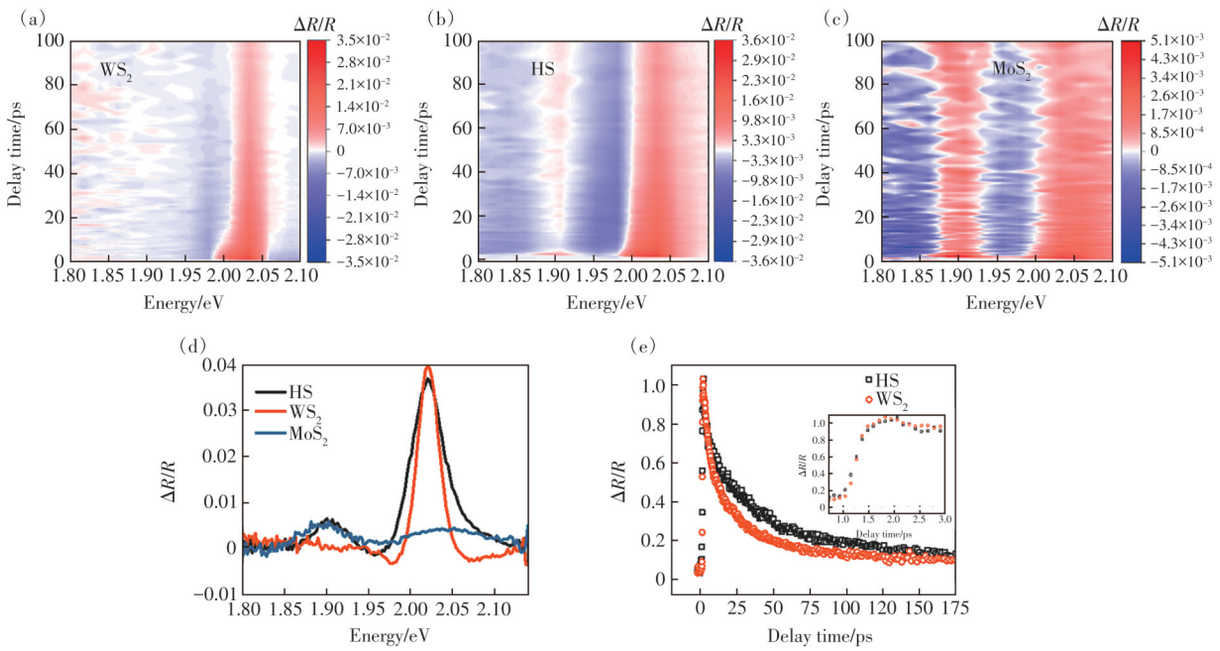

Fig. 3　2D color plot of TA spectra for individual 1L WS_2(a), 1L-MoS_2/hBN/1L-WS_2 HS(b) and individual 1L MoS_2(c). (d) TA spectra of individual 1L WS_2, individual 1L MoS_2 and 1L-MoS_2/hBN/1L-WS_2 HS after the delay time of 2.1 ps, respectively. (e) Normalized decay curves of A exciton of individual 1L WS_2 and that in the HS. Inset is a magnification of Fig.3(e) for the first 3.0 ps

Fig. 3(e) presents normalized decay curves of A exciton of individual 1L WS_2 and that in the 1L-MoS_2/hBN/1L-WS_2 HS extracted at 2.02 eV. Meanwhile, the buildup of exciton populations happens within ~ 1 ps as shown in the inset of Fig. 3(e), which is close to the time resolution of our setup. The GSB signal of A exciton of 1L WS_2 in the HS region is slightly higher than that in its individual region, and this difference could be larger in different samples (Fig. S7), suggesting that interlayer FRET happens in a ps timescale. More interestingly, the FRET process lasts more than one hundred ps in Fig. 3(e). The decay dynamics are well fitted with a biexponential decay function $A_1e^{-t/\tau_1} + A_2e^{-t/\tau_2}$ (see Fig. S8 and Tab. S1 for more details).

For individual 1L WS_2, τ_1 and τ_2 are 5.17 ps and 41.6 ps, respectively. In comparison, τ_1 and τ_2 are 5.19 ps and 60.7 ps, respectively, for 1L WS_2 in the HS. The fast decay component (τ_1) is identical and attributed to intrinsic radiative lifetime of excitons in 1L WS_2[46-47], as shown in Fig. 4(a). The slow decay component (τ_2) in individual 1L WS_2 arises from the Auger-type EEA process[48]. The EEA is a nonradiative scattering process, in which one exciton recombines nonradiatively by transferring its energy and momentum to another exciton, and thus generating hot electron and hole at higher energy level shown in Fig. 4(b). The EEA process is efficient due to strongly enhanced Coulomb interaction in 1L TMDs[49]. Those EEA-generated hot electrons and holes could relax down and form A and B excitons again. Therefore, we believe that the longer τ_2 for 1L WS_2 in the HS is caused by EEA assisted FRET as illustrated in Fig. 4(b).

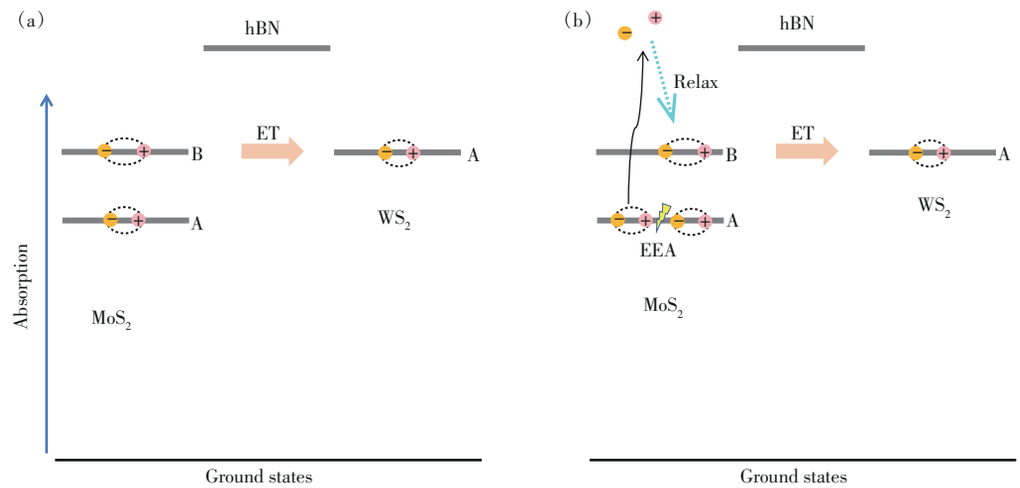

Fig. 4 The schematic illustration of fast interlayer FRET process(a) and slow EEA assisted FRET(b) in 1L-MoS_2/hBN/1L-WS_2 HS. EEA can happen for A/B excitons and even dark excitons in monolayer TMDs, and generates hot carriers at high energy levels which could relax down and form A/B excitons. The EEA-regenerated B excitons in 1L MoS_2 could transfer their energy to A excitons in 1L WS_2 repeatedly, resulting a longer τ_2 for 1L WS_2 in the HS

We further prepared 2L-MoS_2/hBN/1L-WS_2 and 3L-MoS_2/hBN/1L-WS_2 to justify the robustness of FRET induced PL enhancement. The thickness of the hBN spacer layer is ~ 10 nm in Fig. S9. The absorption peaks of A exciton of 1L, 2L, and 3L MoS_2 are located at 1.89, 1.87, 1.84 eV, respectively, as shown in Fig. 5 (a). The PL peak of 1L MoS_2 A exciton is located at 1.89 eV in Fig. S10. For 2L and 3L MoS_2, the PL peaks of the indirect bandgap are stronger than those of A excitons in Fig. S10, which located at 1.86 eV, and the peak at 1.58 eV and 1.43 eV, respectively. The absorption peaks of B excitons of 1L, 2L and 3L MoS_2 are located at about 2.03 eV and show weak dependence on their thickness. The PL enhancement of 1L WS_2 in 2L-MoS_2/hBN/1L-WS_2 and 3L-MoS_2/hBN/1L-WS_2 HSs is observed with EFs of ~2 as shown in Fig. 5(b). 2L and 3L MoS_2 are indirect bandgap semiconductors, and thus photogenerated carriers are more inclined to relax to the indirect bandgap edge and recombine. However, as evidenced by the PL spectra in Fig. S10, a certain population of B excitons can still form in 2L and 3L MoS_2, whose energy can transfer to 1L WS_2 in the HSs through interlayer FRET, and therefore leading to the PL enhancement effect in Fig. 5(b).

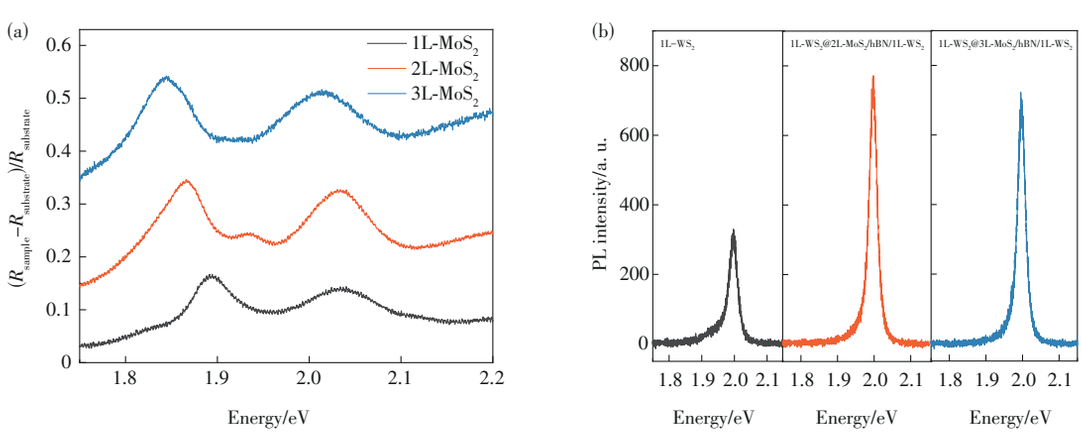

Fig. 5 (a) The differential reflectance spectra of 1L, 2L and 3L MoS_2 at room temperature. (b) PL spectra of A exciton of 1L WS_2 in individual 1L WS_2 (left), in 2L-MoS_2/hBN/1L-WS_2 HS (middle) and in 3L-MoS_2/hBN/1L-WS_2 HS (right)

4 Conclusion

In summary, our study demonstrates an efficient interlayer FRET process from 1L MoS_2 to 1L WS_2 in 1L-MoS_2/hBN/1L-WS_2 HSs, which leads to a significant PL enhancement of 1L WS_2. The interlayer FRET process happened in a picosecond timescale as revealed by transient absorption spectroscopy, since the strong spectral overlap and dipole-dipole interaction between B excitons of 1L MoS_2 and A excitons of 1L WS_2. Importantly, we found that exciton-exciton annihilation plays a critical role in enhancing the interlayer FRET at a timescale of around one hundred picoseconds. Our findings pave a new way to regulate the emission properties of 2D TMDs and provide more insight into the dynamics of interlayer FRET in TMDs HSs.

Supplementary Information and Response Letter are available for this paper at: http://cjl.lightpublishing.cn/thesisDetails#10.37188/CJL.20240238

References:

[1] 常诚, 陈伟, 陈也, 等. 二维材料最新研究进展[J]. 物理化学学报, 2021, 37(12): 2108017.
CHANG C, CHEN W, CHEN Y, *et al*. Recent progress on two-dimensional materials [J]. *Acta Phys. -Chim. Sinica*, 2021, 37(12): 2108017. (in Chinese)

[2] MAK K F, SHAN J. Photonics and optoelectronics of 2D semiconductor transition metal dichalcogenides [J]. *Nat. Photon.*, 2016, 10(4): 216-226.

[3] 孙俊杰, 陈飞, 何洋, 等. 新型过渡金属硫化物在超快激光中的应用[J]. 中国光学, 2020, 13(4): 647-659.
SUN J J, CHEN F, HE Y, *et al*. Application of emerging transition metal dichalcogenides in ultrafast lasers [J]. *Chin. Opt.*, 2020, 13(4): 647-659. (in Chinese)

[4] CUI X, LEE G H, KIM Y D, *et al*. Multi-terminal transport measurements of MoS_2 using a van der Waals heterostructure device platform [J]. *Nat. Nanotechnol.*, 2015, 10(6): 534-540.

[5] LOPEZ-SANCHEZ O, LEMBKE D, KAYCI M, *et al*. Ultrasensitive photodetectors based on monolayer MoS_2 [J]. *Nat. Nanotechnol.*, 2013, 8(7): 497-501.

[6] 何嘉玉, 陈克强, 冀婷, 等. 基于二维材料的快速响应金属-半导体-金属结构光电探测器研究进展[J]. 发光学报, 2022, 43(5): 745-762.
HE J Y, CHEN K Q, JI T, *et al*. Research progress of fast response 2D material photodetectors with metal-semiconductor-metal structure [J]. *Chin. J. Lumin.*, 2022, 43(5): 745-762. (in Chinese)

[7] 夏风梁, 石凯熙, 赵东旭, 等. 二维WSe_2场效应晶体管光电性能[J]. 发光学报, 2021, 42(2): 257-263.
XIA F L, SHI K X, ZHAO D X, *et al*. Optoelectronic performance of 2D WSe_2 field effect transistor [J]. *Chin. J. Lumin.*, 2021, 42(2): 257-263. (in Chinese)

[8] XIAO D, LIU G B, FENG W X, *et al*. Coupled spin and valley physics in monolayers of MoS_2 and other group-VI dichalcogenides [J]. *Phys. Rev. Lett.*, 2012, 108(19): 196802.

[9] MAK K F, HE K L, LEE C, *et al*. Tightly bound trions in monolayer MoS_2 [J]. *Nat. Mater.*, 2013, 12(3): 207-211.

[10] ROSS J S, WU S F, YU H Y, *et al*. Electrical control of neutral and charged excitons in a monolayer semiconductor [J]. *Nat. Commun.*, 2013, 4(1): 1474.

[11] MOURI S, MIYAUCHI Y, MATSUDA K. Tunable photoluminescence of monolayer MoS_2 *via* chemical doping [J]. *Nano Lett.*, 2013, 13(12): 5944-5948.

[12] KOPERSKI M, MOLAS M R, ARORA A, *et al*. Optical properties of atomically thin transition metal dichalcogenides: observations and puzzles [J]. *Nanophotonics*, 2017, 6(6): 1289-1308.

[13] MAN M K L, MADÉO J, SAHOO C, *et al*. Experimental measurement of the intrinsic excitonic wave function [J]. *Sci. Adv.*, 2021, 7(17): eabg0192.

[14] SPLENDIANI A, SUN L, ZHANG Y B, *et al*. Emerging photoluminescence in monolayer MoS_2 [J]. *Nano Lett.*, 2010, 10(4): 1271-1275.

[15] POELLMANN C, STEINLEITNER P, LEIERSEDER U, *et al*. Resonant internal quantum transitions and femtosecond radiative decay of excitons in monolayer WSe_2 [J]. *Nat. Mater.*, 2015, 14(9): 889-893.

[16] LEE Y, KIM J. Controlling lattice defects and inter-exciton interactions in monolayer transition metal dichalcogenides for efficient light emission [J]. *ACS Photonics*, 2018, 5(11): 4187-4194.

[17] WANG H N, ZHANG C J, RANA F. Ultrafast dynamics of defect-assisted electron-hole recombination in monolayer MoS_2 [J]. *Nano Lett.*, 2015, 15(1): 339-345.

[18] 王云坤, 李耀龙, 高宇南. 二维过渡金属硫族化合物中的缺陷和相关载流子动力学的研究进展 [J]. 中国光学, 2021, 14(1): 18-42.
WANG Y K, LI Y L, GAO Y N. Progress on defect and related carrier dynamics in two-dimensional transition metal chalcogenides [J]. *Chin. Opt.*, 2021, 14(1): 18-42. (in Chinese)

[19] KIM Y, KIM J. Near-field optical imaging and spectroscopy of 2D-TMDs [J]. *Nanophotonics*, 2021, 10(13): 3397-3415.

[20] SUN D Z, RAO Y, REIDER G A, *et al*. Observation of rapid exciton-exciton annihilation in monolayer molybdenum disulfide [J]. *Nano Lett.*, 2014, 14(10): 5625-5629.

[21] YUAN L, HUANG L B. Exciton dynamics and annihilation in WS_2 2D semiconductors [J]. *Nanoscale*, 2015, 7(16): 7402-7408.

[22] COURTADE E, SEMINA M, MANCA M, *et al*. Charged excitons in monolayer WSe_2: experiment and theory [J]. *Phys. Rev.* B, 2017, 96(8): 085302.

[23] QIU D Y, JORNADA F HDA, LOUIE S G. Optical spectrum of MoS_2: many-body effects and diversity of exciton states [J]. *Phys. Rev. Lett.*, 2013, 111(21): 216805.

[24] NOVOSELOV K S, JIANG D, SCHEDIN F, *et al*. Two-dimensional atomic crystals [J]. *Proc. Natl. Acad. Sci. USA*, 2005, 102(30): 10451-10453.

[25] LIU K K, ZHANG W J, LEE Y H, *et al*. Growth of large-area and highly crystalline MoS_2 thin layers on insulating substrates [J]. *Nano Lett.*, 2012, 12(3): 1538-1544.

[26] AMANI M, LIEN D H, KIRIYA D, *et al*. Near-unity photoluminescence quantum yield in MoS_2 [J]. *Science*, 2015, 350(6264): 1065-1068.

[27] KIM H, UDDIN S Z, HIGASHITARUMIZU N, *et al*. Inhibited nonradiative decay at all exciton densities in monolayer semiconductors [J]. *Science*, 2021, 373(6553): 448-452.

[28] LEE Y, GHIMIRE G, ROY S, *et al*. Impeding exciton-exciton annihilation in monolayer WS_2 by laser irradiation [J]. *ACS Photonics*, 2018, 5(7): 2904-2911.

[29] HOSHI Y, KURODA T, OKADA M, *et al*. Suppression of exciton-exciton annihilation in tungsten disulfide monolayers encapsulated by hexagonal boron nitrides [J]. *Phys. Rev.* B, 2017, 95(24): 241403.

[30] ZIPFEL J, KULIG M, PEREA-CAUSÍN R, *et al*. Exciton diffusion in monolayer semiconductors with suppressed disorder [J]. *Phys. Rev.* B, 2020, 101(11): 115430.

[31] TANOH A O A, ALEXANDER-WEBBER J, FAN Y, *et al*. Giant photoluminescence enhancement in $MoSe_2$ monolayers treated with oleic acid ligands [J]. *Nanoscale Adv.*, 2021, 3(14): 4216-4225.

[32] KIM M S, ROY S, LEE J, *et al*. Enhanced light emission from monolayer semiconductors by forming heterostructures with ZnO thin films [J]. *ACS Appl. Mater. Interfaces*, 2016, 8(42): 28809-28815.

[33] HU Z H, HERNÁNDEZ-MARTÍNEZ P L, LIU X, *et al*. Trion-mediated Förster resonance energy transfer and optical gating effect in WS_2/hBN/$MoSe_2$ heterojunction [J]. *ACS Nano*, 2020, 14(10): 13470-13477.

[34] KARMAKAR A, AL-MAHBOOB A, PETOUKHOFF C E, *et al*. Dominating interlayer resonant energy transfer in type-Ⅱ 2D heterostructure [J]. *ACS Nano*, 2022, 16(3): 3861-3869.

[35] HU Z H, LIU X, HERNÁNDEZ-MARTÍNEZ P L, *et al*. Interfacial charge and energy transfer in van der Waals heterojunctions [J]. *InfoMat*, 2022, 4(3): e12290.

[36] HU Z H, KRISNANDA T, FIERAMOSCA A, *et al*. Energy transfer driven brightening of MoS_2 by ultrafast polariton relaxation in microcavity MoS_2/hBN/WS_2 heterostructures [J]. *Nat. Commun.*, 2024, 15(1): 1747.

[37] DANDU M, WATANABE K, TANIGUCHI T, *et al*. Spectrally tunable, large Raman enhancement from nonradiative energy transfer in the van der Waals heterostructure [J]. *ACS Photonics*, 2020, 7(2): 519-527.

[38] ZHAO W J, GHORANNEVIS Z, CHU L Q, *et al*. Evolution of electronic structure in atomically thin sheets of WS_2 and WSe_2 [J]. *ACS Nano*, 2013, 7(1): 791-797.

[39] DHAKAL K P, DUONG D L, LEE J, *et al*. Confocal absorption spectral imaging of MoS_2: optical transitions depending on the atomic thickness of intrinsic and chemically doped MoS_2 [J]. *Nanoscale*, 2014, 6(21): 13028-13035.

[40] RAJA A, CHAVES A, YU J, *et al*. Coulomb engineering of the bandgap and excitons in two-dimensional materials [J]. *Nat. Commun.*, 2017, 8(1): 15251.

[41] RIGOSI A F, HILL H M, LI Y L, *et al*. Probing interlayer interactions in transition metal dichalcogenide heterostructures by optical spectroscopy: MoS_2/WS_2 and $MoSe_2$/WSe_2 [J]. *Nano Lett.*, 2015, 15(8): 5033-5038.

[42] ZHOU H Z, ZHAO Y D, TAO W J, *et al*. Controlling exciton and valley dynamics in two-dimensional heterostructures with atomically precise interlayer proximity [J]. *ACS Nano*, 2020, 14(4): 4618-4625.

[43] LEE Y, FORTE J D S, CHAVES A, *et al*. Boosting quantum yields in two-dimensional semiconductors *via* proximal metal plates [J]. *Nat. Commun.*, 2021, 12(1): 7095.

[44] 许文雄, 张何, 崔乾楠, 等. 二维半导体的相干声学声子研究进展 [J]. 发光学报, 2024, 45(8): 1232-1246.
XU W X, ZHANG H, CUI Q N, *et al*. Research progress of coherent acoustic phonons in two-dimensional semiconductors [J]. *Chin. J. Lumin.*, 2024, 45(8): 1232-1246. (in Chinese)

[45] HE Z Y, ZHAO R, CHEN X F, *et al*. Defect engineering in single-layer MoS_2 using heavy ion irradiation [J]. *ACS Appl. Mater. Interfaces*, 2018, 10(49): 42524-42533.

[46] ZHAO J X, ZHAO W J, Du W, *et al*. Dynamics of exciton energy renormalization in monolayer transition metal disulfides [J]. *Nano Res.*, 2020, 13(5): 1399-1405.

[47] ROBERT C, LAGARDE D, CADIZ F. Exciton radiative lifetime in transition metal dichalcogenide monolayers [J]. *Phys. Rev.* B, 2016, 93(20): 205423.

[48] STEINLEITNER P, MERKL P, NAGLER P, *et al*. Direct observation of ultrafast exciton formation in a monolayer of WSe_2 [J]. *Nano Lett.*, 2017, 17(3): 1455-1460.

[49] LINARDY E, YADAV D, VELLA D, *et al*. Harnessing exciton-exciton annihilation in two-dimensional semiconductors [J]. *Nano Lett.*, 2020, 20(3): 1647-1653.

陈朋尧(1999-),女,河南洛阳人,硕士研究生,2021年于河南师范大学获得学士学位,主要从事二维过渡金属硫族化合物光学性质的研究。
E-mail: cpy-123@seu.edu.cn

赵伟杰(1982-),男,山东烟台人,博士,教授,博士生导师,2011年于中国科学院半导体研究所获得博士学位,主要从事二维光电材料与器件的研究。
E-mail: zhaowj@seu.edu.cn